Bioorganic Chemistry 179 (2026) 109993

Contents lists available at ScienceDirect

Bioorganic Chemistry

journal homepage: www.elsevier.com/locate/bioorg

A target-directed platform for identification of ligands of *Schistosoma mansoni* methylthioadenosine phosphorylase in natural product extracts

Lucas G. do Amaral [a], Miguel F.S. de Abreu [a], Renato C.S. Lessa [a,b], Pamella C.O. de Oliveira [a], Magali S. Amorim [a], Jorge L.S. Simão [c], Martin Albino [d,e], Humberto d'Muniz Pereira [f], Claudio Sangregorio [d,e], Vanessa G.P. Severino [c], Marcela C. de Moraes [a,*]

[a] *BioCrom, Organic Chemistry Department, Chemistry Institute, Fluminense Federal University, 24020-141 Niterói/RJ, Brazil*
[b] *Institute of Chemistry, Organic Chemistry Department, Rio de Janeiro State University, Rio de Janeiro/RJ 20550-013, Brazil*
[c] *Institute of Chemistry, Federal University of Goiás, Campus Samambaia, Esperança avenue, 74690900 Goiânia/Go, Brazil*
[d] *ICCOM-CNR, 50019 Sesto Fiorentino (FI), Italy*
[e] *Department of Chemistry 'Ugo Schiff', University of Florence and INSTM, 50019 Sesto Fiorentino (FI), Italy*
[f] *São Carlos Institute of Physics, University of São Paulo, 13566-590 São Carlos/SP, Brazil*

ARTICLE INFO

Keywords:
Enzyme immobilization
Magnetic nanoparticle
High-performance liquid chromatography
Natural products
Schistosomiasis
Drug discovery

ABSTRACT

5′-Methylthioadenosine phosphorylase from *Schistosoma mansoni* (*Sm*MTAP) is a promising target within the parasite's purine salvage pathway. In this study, *Sm*MTAP was covalently immobilized onto amine-functionalized cobalt ferrite magnetic nanoparticles ($CoFe_2O_4$), generating a reusable bioreactor ($CoFe_2O_4$@*Sm*MTAP) with an immobilization efficiency of 66.3 ± 6.6%. Enzymatic activity was monitored by HPLC-DAD through the direct quantification of adenine using a validated analytical method (linearity 1–100 μmol/L, $R^2 = 0.9999$; LOD 0.005 μmol/L; LOQ 0.01 μmol/L). The immobilized enzyme displayed Michaelis-Menten behavior (apparent K_M = 29.45 ± 7.34 μmol/L), retained more than 60% residual activity over two weeks, and preserved more than 50% activity after seven reaction cycles. The platform was applied to the screening of eight natural product extracts, identifying the ethanolic stem extract from *Hymenaea stigonocarpa* as a potential source of *Sm*MTAP inhibitors (IC_{50} = 8.29 ± 0.94 μg/mL). Affinity selection–mass spectrometry (AS-MS) with $CoFe_2O_4$@*Sm*MTAP revealed six putative ligands (affinity ratios 1.45–2.89) in the crude extract. Analytical-scale microfractionation was conducted, specifically targeting the retention time windows of the ligands previously detected by AS-MS. This strategy successfully localized the main bioactive region to the 30.75–33.0 min window, which overlaps with the retention times of two ligands, including a compound tentatively annotated as asperphenamate. Complementary UHPLC–HRMS dereplication enabled the putative annotation of 23 compounds. Overall, the integrated workflow provided a selective, material-efficient, and reusable bioanalytical platform for screening *Sm*MTAP inhibitors in complex natural libraries.

1. Introduction

Schistosomiasis remains one of the most devastating neglected tropical diseases (NTDs), with *Schistosoma mansoni* causing chronic infections in approximately 251 million people across more than 70 countries and threatening an additional 800 million individuals in regions characterized by poor sanitation and limited economic development [1,2]. As the largest endemic area in the Americas, Brazil has an estimated 1.5 million people at risk, particularly in the Northeast and Southeast regions where *Biomphalaria* snails act as intermediate hosts [3]. Between 2009 and 2019, the Brazilian Schistosomiasis Control Program identified 423,117 new cases with an average positivity rate of 4.29% [3,4]. Despite this substantial disease burden, therapeutic options remain severely limited.

Current treatment relies almost exclusively on praziquantel and oxamniquine, drugs that have been in clinical use for over 50 years [5]. Both agents cause significant adverse effects and are associated with high recurrence rates due to incomplete parasite clearance and emerging drug resistance [6,7]. No vaccine is currently available, underscoring the urgent need for novel therapeutic approaches that exploit

* Corresponding author at: Marcela Cristina de Moraes, Organic Chemistry Department, Chemistry Institute, Fluminense Federal University, Niterói/RJ, Brazil.
E-mail address: mcmoraes@id.uff.br (M.C. de Moraes).

https://doi.org/10.1016/j.bioorg.2026.109993
Received 19 March 2026; Received in revised form 1 May 2026; Accepted 14 May 2026
Available online 15 May 2026

Schistosoma-specific metabolic vulnerabilities.

A particularly promising target lies within the parasite's unique purine metabolism. Studies by Senft and colleagues (1970s–1980s) [8,9] and Dovey et al. [10] established that *S. mansoni* completely lacks the de novo pathway for purine biosynthesis, depending exclusively on the salvage pathway to acquire essential nitrogenous bases such as adenine (ADE) for DNA, RNA, and ATP production [11–13]. Within this pathway, 5′-deoxy-5′-methylthioadenosine phosphorylase (*Sm*MTAP) plays a critical role in generating ADE from adenosine (ADO) [10,11,14]. Importantly, humans possess alternative pathways for ADE acquisition, making *Sm*MTAP an attractive target for selective, non-toxic drug development [15]. Despite this therapeutic potential, only one *Sm*MTAP inhibitor has been described in the literature [16], 5′-deoxy-5′-chloroformycin A.

Traditional methods for screening enzyme inhibitors present substantial limitations that hinder drug discovery efforts. Spectrophotometric assays, while convenient, often generate false positives due to interference from complex matrices such as natural product libraries. Coupled enzymatic assays introduce additional sources of error, as secondary enzymes may themselves be inhibited by test compounds. Furthermore, conventional approaches require substantial quantities of purified enzyme, creating significant cost barriers when working with recombinant proteins. The increasing demand for high-throughput screening in modern drug discovery programs necessitates innovative methodological solutions that address these challenges.

Enzyme immobilization on magnetic nanoparticles offers a paradigm shift in bioanalytical methodology, enabling enzyme reuse, simplified magnetic separation, enhanced stability, and integration with automated systems [17,18]. Among magnetic materials, cobalt ferrite ($CoFe_2O_4$) nanoparticles exhibit exceptional properties including high magnetic saturation, chemical stability, and facile surface functionalization, making them ideal supports for enzyme immobilization [19]. When integrated into high-performance liquid chromatography (HPLC) systems, immobilized enzyme reactors (IMERs) provide direct quantification of enzymatic products, eliminating interferences and false positives inherent to alternative detection methods [20,21]. However, the application of immobilized *Sm*MTAP for high-efficiency natural product screening remains unexplored, representing a critical knowledge gap in anti-schistosomal drug discovery.

Natural products remain invaluable sources of pharmaceutical leads, with many current drugs, including morphine, artemisinin, taxol, and hypericin, derived from natural sources [22–25]. The chemical and pharmacological diversity of plant secondary metabolites makes them especially attractive for the discovery of novel enzyme inhibitors. However, the investigation of natural products as sources of bioactive compounds often involves labor-intensive fractionation and purification processes or requires the use of sophisticated analytical platforms capable of correlating biological activity with chemical composition. In this context, combining affinity selection-mass spectrometry (AS-MS), which directly identifies potential ligands in crude extracts, with analytical-scale microfractionation provides a powerful dual approach to identify bioactive structures with complex libraries.

The present study addresses a critical gap in the field by reporting, for the first time, a direct activity-based assay for *Sm*MTAP. The only enzymatic assay previously described in the literature relies on a coupled spectrophotometric method employing xanthine oxidase as an auxiliary enzyme [26]. Such coupled approaches introduce additional sources of variability and potential false positives, particularly when screening complex mixtures, as the auxiliary enzyme may itself be inhibited by extract components. To overcome this limitation, *Sm*MTAP was covalently immobilized onto $CoFe_2O_4$ magnetic nanoparticles, and its catalytic activity was monitored through a direct HPLC-UV method, providing an interference-free basis for inhibitor screening. Moreover, while the use of magnetic IMERs for AS-MS has been explored for related enzymes, including nucleoside hydrolase from *Leishmania donovani* [27,28], its application to *Sm*MTAP represents a critical and previously unexplored opportunity in anti-schistosomal drug discovery. Most distinctively at the workflow level, this is the first study in which analytical-scale microfractionation is strategically directed to the retention time windows of ligands previously captured by AS-MS, enabling a more material-efficient and hypothesis-driven correlation between binding affinity and functional inhibition. In this context, this study reports the development of a $CoFe_2O_4$@*Sm*MTAP-based IMER platform integrating AS-MS with targeted microfractionation for the discovery of *Sm*MTAP inhibitors from natural product extracts.

2. Experimental

2.1. Chemicals and reagents

Dimethyl sulfoxide (DMSO, ≥99.7%, HPLC grade), glutaraldehyde solution (GA, 25% *v*/v in H_2O), hydrochloric acid (HCl, P.A.), formic acid (P.A.), pyridine (≥99%), glycine (Gly, ≥99%), adenine (ADE, ≥99%), adenosine (ADO, ≥99%), anhydrous dibasic potassium phosphate (K_2HPO_4, ≥98%), ammonium acetate (NH_4OAc, HPLC grade), tris (hydroxymethyl)aminomethane (Tris, P.A.), 6-aminohexyl phosphonic acid (AEPA, ≥ 95%), oleic acid (OA, 90%), oleylamine (ONH_2, ≥ 98%), and dibenzyl ether (Bz_2O, 99%) were obtained from Sigma-Aldrich (St. Louis, USA). Cobalt (II) acetylacetonate ($Co(acac)_2$, 99%) and iron (III) acetylacetonate ($Fe(acac)_3$, 99%) were obtained from Strem Chemicals (Newburyport, USA). The mobile phase was prepared using methanol (MeOH,) and acetonitrile (ACN) (HPLC grade) from J.T. Baker (Xalostoc, Mexico). Analytical columns Supelco Discovery C-18 (5 µm, 50 × 4.6 mm) and Supelco Ascentis C18 (5 µm, 250 × 4.6 mm) were obtained from Sigma-Aldrich (St. Louis, USA).

Ultrapure Type I water was obtained from a Milli-Q Reference system (Millipore, São Paulo, Brazil) for preparation of all aqueous solutions. Buffer solutions were filtered through 0.22 µm membrane filters (Merck Millipore) prior to analysis.

2.2. Instrumentation and software

*Sm*MTAP activity assays and inhibitor screening were performed using a Shimadzu Nexera XR liquid chromatography system (Kyoto, Japan) equipped with a DAD detector (SPD-M20A0 and LabSolutions v.5.84 software. UHPLC-HRMS analyses for dereplication and AS-MS were conducted at the Biomolecular Mass Spectrometry Center (CEMBIO) of the Federal University of Rio de Janeiro using a Shimadzu Nexera X2 ultra-high-performance liquid chromatography system (Kyoto, Japan) coupled to a Bruker Daltonics Impact HD high-resolution mass spectrometer (Massachusetts, USA). The mass spectrometer featured an electrospray ionization (ESI) source and a quadrupole time-of-flight (Q-TOF) hybrid mass analyzer. Quantification of immobilized enzyme was performed using a Jasco V-730 Bio UV–Vis spectrophotometer.

2.3. SmMTAP expression and purification

Recombinant *Sm*MTAP was expressed in *Escherichia coli* and purified using established protocols [26]. Briefly, protein expression was carried out in 1 L of 2 × YT medium supplemented with 50 µg/mL kanamycin. Overnight cultures were inoculated and grown at 37 °C until reaching $OD_{600} \approx 0.6$. Protein expression was induced with 0.1 mmol/L isopropyl β-D-thiogalactopyranoside (IPTG) for 4 h at 37 °C. Cells were harvested by centrifugation (6000 ×*g*, 45 min, 4 °C) and lysed by sonication in buffer containing 50 mmol/L NaH_2PO_4 (pH 7.4), 300 mmol/L NaCl, 10 mmol/L imidazole, and 5 mmol/L β-mercaptoethanol. The lysate was clarified by centrifugation (9000 ×*g*, 20 min, 4 °C), and the soluble fraction was applied to a Co-NTA agarose column (Clontech). Following washing with buffer containing 50 mmol/L NaH_2PO_4 (pH 7.4), 300 mmol/L NaCl, 20 mmol/L imidazole, and 5 mmol/L β-mercaptoethanol, the enzyme was eluted with buffer containing 50 mmol/L NaH_2PO_4 (pH

7.4), 300 mmol/L NaCl, 200 mmol/L imidazole, and 5 mmol/L β-mercaptoethanol. The purified enzyme was dialyzed against 20 mmol/L Tris (pH 7.4), 200 mmol/L NaCl, and 10 mmol/L β-mercaptoethanol. The final *Sm*MTAP solution (1.8 mg/mL) was stored at −80 °C with 20% glycerol.

Access to genetic heritage for recombinant *S. mansoni* MTAP was registered in the National System for the Management of Genetic Heritage and Associated Traditional Knowledge (SisGen) under code AF84B09.

2.4. Synthesis and characterization of $CoFe_2O_4$ nanoparticles

$CoFe_2O_4$ magnetic nanoparticles functionalized with amine groups were synthesized using a modified thermal decomposition method previously reported [19]. The procedure involved dissolving 8 mmol of metal precursors, $Fe(acac)_3$ and $Co(acac)_2$, in a 2:1 M ratio, in a solution containing 24 mmol OA, 24 mmol ONH_2, and 60 mL Bz_2O in a 100 mL three-neck round-bottom flask. The mixture was heated to 300 °C under continuous N_2 flow for 1.5 h. The flask was removed from the heating mantle and allowed to cool under an inert atmosphere. Nanoparticles were purified through multiple cycles of ethanol-induced coagulation, removal of the supernatant, and redispersion in toluene for storage.

Amino functionalization was achieved by replacing the OA surface coating with AEPA. Nanoparticles were resuspended in 20 mL chloroform at a 1:1 (*w*/w) ratio with AEPA and mixed with 5 mL of AEPA solution in DMSO. The suspension was subjected to ultrasonic bath treatment for 40 min, followed by gentle stirring for 20 h. Amino-functionalized $CoFe_2O_4$ nanoparticles were washed twice with DMSO and once with EtOH, then stored in water until use.

For the $CoFe_2O_4$ nanoparticles characterization, elemental composition was determined by energy-dispersive X-ray spectroscopy (EDX). The morphology and size distribution were assessed by Transmission electron microscopy (TEM) micrographs, while the spinel structure and phase purity were confirmed by Powder X-ray diffraction (PXRD) patterns. Elemental analysis (C, H, N) was used to verify the AEPA functionalization. Magnetic response was determined using a superconducting quantum interference device (SQUID) magnetometer.

2.5. Immobilization of SmMTAP onto $CoFe_2O_4$ ($CoFe_2O_4$@SmMTAP)

For the immobilization, 2.5 mg of $CoFe_2O_4$ nanoparticles were washed three times with coupling buffer (10 mmol/L pyridine, pH 6.0). Particles were then incubated with 500 µL of 5% *v*/v glutaraldehyde in coupling buffer, vortexed for 30 s, and maintained on an orbital shaker for 3 h at 21 °C. After magnetic separation (1 min), the supernatant was removed and particles were washed five times with coupling buffer.

Subsequently, 0.5 mg of *Sm*MTAP in 100 mmol/L phosphate buffer (pH 7.4) was added to the activated particles, vortexed for 30 s, and incubated on an orbital shaker for 4 h at 4 °C. Following incubation, the supernatant was collected after magnetic separation (1 min) and stored at −20 °C for enzyme quantification and immobilization yield determination. Unreacted aldehyde groups were blocked by adding 500 µL of glycine solution (1.0 mol/L, pH 8.0), vortexing for 30 s, and incubating for 30 min at 4 °C under orbital agitation. After magnetic separation, 1.0 mL of Tris buffer (100 mmol/L, pH 7.4) was added, followed by 1:5 dilution with the same buffer. The final suspension contained cobalt ferrite magnetic nanoparticles with immobilized *Sm*MTAP ($CoFe_2O_4$@*Sm*MTAP) at 500 µg/mL.

Enzyme concentrations before and after immobilization were determined in quintuplicate using UV spectrophotometry at 280 nm. The molar extinction coefficient (ε = 29,450 L mol^{-1} cm^{-1}) was calculated according to Gill and von Hippel (1989) [29]. Immobilization efficiency (IE) was determined using Eq. 1.

$$IE\ (\%) = \left(\frac{C_0 - C_S}{C_S}\right) \times 100 \quad (1)$$

where C_0 = initial concentration of *Sm*MTAP in solution before immobilization (mg/mL), C_S = concentration of *Sm*MTAP in the supernatant after immobilization (mg/mL), and IE = immobilization efficiency.

2.6. HPLC-DAD method and qualification

Enzymatic activity was monitored by quantifying ADE formation in *Sm*MTAP-catalyzed reactions using HPLC-DAD. ADO and ADE chromatographic separation was conducted on a Supelco Discovery C18 analytical column (5 µm, 50 × 4.6 mm) with isocratic elution. The mobile phase consisted of ammonium acetate solution (20 mmol/L, pH 6.0) and acetonitrile at a ratio of 95:5 (*v*/v) with a flow rate of 0.8 mL/min [30]. The injection volume was 20 µL, and analytes were monitored at 260 nm.

The analytical method was qualified by assessing selectivity, linearity, precision, accuracy, limit of detection (LOD) and limit of quantification (LOQ) [31]. Selectivity was assessed by injecting phosphate buffer (100 mmol/L, pH 7.4) and comparing the chromatogram with that obtained from an equimolar solution (200 µmol/L) of ADO and ADE with respect to retention times and peak overlap. Linearity was evaluated by constructing an analytical calibration curve with ADE concentrations ranging from 1 to 100 µmol/L (1, 2.5, 5, 10, 25, 50, and 100 µmol/L), prepared in triplicate.

Method precision and accuracy were determined intra- and inter-day using quality control solutions prepared in quintuplicate at ADE concentrations of 1.2, 40, and 90 µmol/L. Precision was evaluated through the coefficient of variation (CV%), while accuracy was assessed by percentage recovery. Acceptance criteria were CV% below 15% and recovery between 85% and 115% [32,33]. LOD was established by injecting decreasing concentrations of ADE until a signal-to-noise ratio of 3:1 was obtained. LOQ was determined under the same conditions until the signal-to-noise ratio reached 10:1.

2.7. Optimization of bioreactor catalytic conditions

$CoFe_2O_4$@*Sm*MTAP activity was assessed using an off-line chromatographic method. To optimize immobilized enzyme activity, different support masses (5, 10, and 25 µg) were tested. The reaction mixture contained $CoFe_2O_4$@*Sm*MTAP, phosphate buffer (100 mmol/L, pH 7.4), and substrate ADO at 40 µmol/L in a final volume of 200 µL, prepared in triplicate for each condition. The mixture was incubated on an orbital shaker for 10 or 20 min at 21 °C. After incubation, magnetic separation was performed for 1 min, and the supernatant was collected and injected into the HPLC-DAD system for ADE quantification, enabling determination of optimal catalytic configuration.

2.8. Stability, reusability and kinetic assays

$CoFe_2O_4$@*Sm*MTAP was characterized through periodic stability assays to evaluate its activity profile over time. During this period, the stock suspension of $CoFe_2O_4$@*Sm*MTAP, at 500 µg/mL, was stored at 4 °C in tris(hydroxymethyl)aminomethane buffer (100 mmol/L, pH 7.4) until use. Catalytic reactions were carried out in triplicate using ADO at 40 µmol/L, 5 µg of $CoFe_2O_4$@*Sm*MTAP, and phosphate buffer (100 mmol/L, pH 7.4) in a final volume of 200 µL. Reactions were incubated for 20 min on an orbital shaker at 21 °C, followed by magnetic separation for 1 min. The supernatant was collected and injected into the HPLC-DAD system. The assay was repeated at periodic time intervals (weeks 0, 1, 2, 4, 5, and 8 after immobilization) to construct the stability profile of the immobilized enzyme.

$CoFe_2O_4$@*Sm*MTAP was characterized by enzymatic kinetics to determine its Michaelis-Menten constant (K_M) and maximum velocity (V_{max}). Increasing concentrations of ADO ranging from 2 to 512 µmol/L (2, 4, 8, 16, 32, 64, 128, 256, and 512 µmol/L) were employed in triplicate. Reactions were conducted under optimized catalytic conditions:

5 μg of $CoFe_2O_4$@*Sm*MTAP, incubation for 20 min on an orbital shaker at 21 °C, followed by 1 min of magnetic separation. The supernatant was injected into the HPLC-DAD system and analyzed under previously described operating conditions for ADE separation and quantification. Experimental data were fitted to a Michaelis-Menten hyperbolic plot ([ADE] versus [ADO]), and K_M and V_{max} values were obtained using GraphPad Prism v.8.0.2 software.

$CoFe_2O_4$@*Sm*MTAP was further characterized through a reusability assay evaluating the activity of immobilized enzyme over ten consecutive reaction cycles. Catalytic conditions were identical to those described in Section 2.7. Between cycles, $CoFe_2O_4$@*Sm*MTAP, initially stored at 500 μg/mL and 4 °C in tris buffer (100 mmol/L, pH 7.4), was washed with 200 μL of phosphate buffer (100 mmol/L, pH 7.4) to remove residual ADE and resuspended in the reaction medium. This procedure was repeated for ten cycles, and the assay was performed in triplicate.

2.9. Plant material and extraction

Hymenaea stigonocarpa Mart. ex Hayne plant material was collected during the flowering stage at the Federal University of Catalão, Catalão, Goiás, Brazil. The species was identified by Prof. Hélder Nagai Consolaro, and a voucher specimen (No. GD 046) was deposited at the Herbarium of EMBRAPA Recursos Genéticos e Biotecnologia. Access to genetic resources was registered in SisGen under code A11AE2. Flowers (HS-EEF), leaves (HS-EEL), roots (HS-EER), stems (HS-EEC), and fruit peel (HS-EECF) were individually macerated with EtOH (3 × 9 L, 3 days each) at room temperature, filtered, and concentrated to yield the crude extracts, as previously described by Monteiro et al. [34].

Moringa oleifera Lam. plant material was collected from a public street in Setor Jaó, Goiânia, Goiás, Brazil. The species was identified by Prof. Aristônio Magalhães Teles. A voucher specimen was deposited at the Herbarium of the Federal University of Goiás (UFG) under number 68186. Access to genetic resources was registered in SisGen under code AB29947. Leaves (MoLV), flowers (MoFL), and stems (MoST) of *M. oleifera* Lam. were dried at room temperature and macerated. Extracts were prepared from different plant parts by infusion extraction using EtOH:H_2O (7:3, v/v) at 90 °C in a bath (SW23 - Julabo), and the mixture was stirred for up to 48 h. Extracts were filtered, concentrated under reduced pressure, and lyophilized to yield dry extracts.

All extracts were solubilized at 5 mg/mL in MeOH, except HS-EEC, which was solubilized in DMSO.

2.10. Inhibitor screening and IC_{50} determination

Inhibitor screening was performed using an off-line reaction to determine the percentage of inhibition exerted by each natural product extract on enzymatic activity. Each extract was tested in triplicate at a concentration of 200 μg/mL, using the catalytic reaction conditions described in section 2.7. The proportion of organic solvent in the reaction was 4% (*v*/v) to avoid significant interference with enzyme activity. Negative controls (blanks) were performed in triplicate by replacing the extract with the corresponding organic solvent. Inhibition percentage was calculated according to eq. 2:

$$Inhibition\ (\%) = \left(\frac{[ADE_{Control}] - [ADE_{Screening}]}{[ADE_{Control}]}\right) \times 100 \quad (2)$$

After supernatant collection following magnetic separation (1 min), samples were injected into the HPLC-DAD system for ADE quantification using the validated chromatographic conditions.

IC_{50} assays were performed for extracts exhibiting inhibition ≥70% in initial screening. Reactions were conducted under the optimized catalytic conditions using increasing extract concentrations from 0.01 to 400 μg/mL. The volume of organic solvent was adjusted to a total of 20 μL, representing 10% of the total reaction volume. Each concentration was tested in triplicate, including the blanks containing only the corresponding organic solvent. After 1 min of magnetic separation, supernatants were collected and analyzed by HPLC-DAD for ADE quantification. Dose-response curves and IC_{50} values were obtained by nonlinear regression using GraphPad Prism v.8.0.2 software.

2.11. Chromatographic profile of *H. stigonocarpa* stem extract

The chromatographic profile of *H. stigonocarpa* stem ethanolic extract (HS-EEC) was optimized using a Supelco Ascentis C-18 analytical column (5 μm, 250 × 4.6 mm). The mobile phase was composed of aqueous solution of 0.1% formic acid (*v*/v) (solvent A) and acetonitrile acidified with 0.1% formic acid (v/v) (solvent B) at a flow rate of 0.8 mL/min. The optimized gradient program was: 0–25 min, 15% B; 25–30 min, 15–55% B; 30–35 min, 55–70% B; 35–40 min, 70–80% B; 40–45 min, 80–96% B; 45–55 min, 96% B; 55–60 min, 96–15% B; 60–70 min, 15% B. An injection volume of 20 μL was used, and samples were monitored at 280 and 365 nm.

2.12. Affinity selection-mass spectrometry (AS-MS)

AS-MS assay used 2.5 mg of freshly prepared $CoFe_2O_4$@*Sm*MTAP incubated with 500 μL of HS-EEC solution (5 mg/mL in 5 mmol/L ammonium acetate buffer, pH 7.4) under orbital shaking for 20 min at 4 °C. Supernatant S_0 (non-ligands) was collected after magnetic separation (3 min). The immobilized enzyme was washed twice with 500 μL of ammonium acetate (5 mmol/L, pH 7.4) followed by 3 min agitation and magnetic separation (3 min), yielding supernatants S_1 and S_2. For the elution step, 500 μL methanol was added to the microtube containing $CoFe_2O_4$@*Sm*MTAP, followed by agitation for 1 h at room temperature and magnetic separation, yielding supernatant S_3. Then 500 μL methanol was added with heating at 60 °C for 1 h, yielding S_4. To distinguish specific from non-specific binding, inactive enzyme controls (pre-treated with methanol for 96 h at room temperature) were processed under identical conditions. This approach was preferred over bare (enzyme-free) nanoparticle controls because the enzyme layer alters the surface chemistry, hydrophobicity, and steric accessibility of the support, so that bare nanoparticles do not accurately replicate the surface environment of the active enzyme assay. The use of denatured, immobilized enzyme controls thus provides a more stringent and representative assessment of target-specific binding versus non-specific adsorption to the support matrix.

Supernatants S_0, S_3, and S_4 from both active and inactive enzyme assays were analyzed by UHPLC-HRMS. Affinity ratios (AR) were calculated:

$$AR = \frac{Peak\ area_{Active\ enzyme}}{Peak\ area_{Inactive\ enzyme}} \quad (3)$$

Compounds with AR > 1.3 were considered ligands, as this threshold ensures a minimum enrichment above non-specific interactions and experimental variability [28].

2.13. AS-MS guided microfractionation and biochromatogram construction

To correlate the chemical features of HS-EEC with biological activity and investigate the inhibitory potential within the retention time windows of the previously identified ligands, analytical-scale microfractionation was performed. The fractionation was strategically directed to the 29.0–44.0 min retention time window, which overlaps with the elution range of six *Sm*MTAP ligands (32.3–41.2 min) captured by AS-MS. HS-EEC (80 mg/mL in DMSO) was injected into the HPLC-DAD system under optimized chromatographic conditions (Section 2.11). Fractions were collected every 15 s (resolution of 4 points/min), yielding a series of 60 microfractions that were subsequently dried using

a SpeedVac. Each fraction was resuspended in the activity assay buffer to determine its inhibitory potential against *Sm*MTAP, following the protocol described in Section 2.10. The inhibition percentages were plotted against their respective retention times to generate the inhibitory profile (biochromatogram).

2.14. UHPLC-HRMS/MS dereplication

For chemical profiling of HS-EEC, a 2 mL solution of extract at 5 mg/mL in 5 mmol/L ammonium acetate (pH 7.4) containing 10% *v*/v DMSO was prepared. A 500 µL aliquot was analyzed by UHPLC-HRMS at CEMBIO-UFRJ.

UHPLC-HRMS conditions included separation on Supelco Ascentis C-18 analytical column (5 µm, 250 × 4.6 mm) with mobile phases consisting of water with 0.1% formic acid (A) and acetonitrile with 0.1% formic acid (B), following the optimized gradient program established in section 2.14. A post-column split maintained a flow rate of 0.3 mL/min into the mass spectrometer source. The LC-MS system includes a Q-TOF (quadrupole time-of-flight) analyzer operating in DDA/AutoMS acquisition mode, with isolation/fragmentation of 5 precursors/cycle, in a scan range of 50–1200 *m/z*, 1 Hz acquisition rate for Full Scan and 2 Hz for DDA, with positive and negative ESI mode, nebulizer set at 4 bar, dry gas at 8 L/min, and dry temperature at 200 °C. The capillary voltage was 3500 V, and the end plate offset at −500 V with quadrupole low mass set at 80 *m/z*. The collision cell energy operated at 6 eV, with a transfer time of 50 µs and 3 µs pre-pulse storage time. Data were analyzed using Compass DataAnalysis (Bruker, Germany).

Raw data were converted to mzxml format and imported into MZmine v.4.9.0 software [35]. Processing included mass detection, chromatogram building, deconvolution, isotopic grouping, alignment, and gap filling (parameters detailed in Table S1). Processed feature lists were exported to GNPS2 [36] for annotation using criteria: cosine score $\geq$ 0.70, m/z difference $\leq$ 0.003 and mass error $\leq$ 10 ppm. Complementary searches used MassBank and PubChem databases.

2.15. Statistical analysis

All experiments were performed at least in triplicate, and results are expressed as mean ± standard deviation (SD). Statistical analyses were performed using GraphPad Prism 8.0 (GraphPad Software, San Diego, CA, USA) and OriginPro 8.5 (OriginLab Corporation, Northampton, MA, USA) software.

Comparisons between experimental groups were evaluated using one-way analysis of variance (ANOVA) followed by Tukey's post-hoc test for multiple comparisons when appropriate. Differences were considered statistically significant at $p < 0.05$.

3. Results and discussion

3.1. Qualification of chromatographic method for ADE quantification

To avoid the spectral interference inherent to spectrophotometric monitoring and the potential for false positives associated with coupled enzymatic assays [37], a direct HPLC-DAD method was established. This approach enables chromatographic resolution of the substrate (ADO) and product (ADE) in a single analysis (Fig. S1).

After establishing chromatographic conditions, the method was qualified to ensure reliable quantification of ADE in enzymatic reactions. Method selectivity was evaluated by injecting samples of phosphate buffer (100 mmol/L, pH 7.4) and comparing the resulting chromatogram with that obtained from standard ADE solutions.

Linearity was assessed by constructing a calibration curve using ADE standard solutions in the concentration range of 1–100 µmol/L. Linear regression of chromatographic peak area against injected ADE concentration (Fig. S2) yielded the equation $y = 18{,}815\times$ - 1400.9 with a determination coefficient (R^2) of 0.9999. Analysis of variance (ANOVA) demonstrated that the regression was statistically significant ($F_{1,16} = 149{,}967.7$; $p < 0.0001$), while the lack-of-fit test was not significant ($F_{5,11} = 0.728$; $p > 0.05$), confirming the adequacy of the linear model.

Intra- and inter-day precision and accuracy were also evaluated (Table 1). Precision, expressed as the coefficient of variation (CV%), ranged from 0.24 to 5.73%, whereas accuracy, expressed as percent recovery, ranged from 96.6 to 107.3%. In this study, precision values below 15% and accuracy values between 85 and 115% were considered acceptable [32,33].

The limit of detection (LOD) was established at 0.005 µmol/L, while the limit of quantification (LOQ) was 0.01 µmol/L. Comparable HPLC-based methods have been described for other nucleoside-metabolizing enzymes, such as purine nucleoside phosphorylase (PNP) [20] and nucleoside hydrolase (NH) [28]. The present method provides a shorter total run time (4 min) than previously reported methods (typically 8–15 min), while maintaining comparable or improved sensitivity. This rapid analysis is particularly advantageous for high-throughput screening applications where a large number of samples must be processed efficiently.

3.2. $CoFe_2O_4$ nanoparticles characterization

The magnetic nanoparticles were characterized using complementary techniques to confirm their composition and suitability for enzyme immobilization and subsequent biological assays. PXRD analysis confirmed the formation of cobalt ferrite nanoparticles, showing a single crystallographic phase consistent with the spinel structure (Fig. S3). The elemental composition determined by EDX revealed weight percentages of 77.86% Fe and 21.33% Co, corresponding to the empirical formula $Co_{0.63}Fe_{2.37}O_4$, which is consistent with the expected cobalt ferrite composition. TEM analysis revealed a mean particle diameter of 29.6 ± 4.04 nm. A representative micrograph is shown in the Supplementary Material (Fig. S4).

Surface functionalization was confirmed by elemental analysis (C, H, N) following ligand exchange. Nitrogen was not detected in the initial $CoFe_2O_4$@OA material, whereas it was detected after modification with AEPA, confirming the successful introduction of amino groups on the nanoparticle surface.

The magnetic response of the nanoparticles was also evaluated. The saturation magnetization values were 81.7 emu/g for $CoFe_2O_4$@AEPA and 83.8 emu/g for $CoFe_2O_4$@AEPA, indicating that the surface modification did not compromise the magnetic properties.

3.3. SmMTAP immobilization and catalysis conditions

Following method qualification, the immobilization and catalytic conditions of *Sm*MTAP were optimized to maximize enzymatic activity.

Two enzyme coupling times were evaluated: 4 h and 16 h, providing immobilized enzyme reactors IMER I and IMER II, respectively. Both IMERs were tested using different masses of $CoFe_2O_4$@*Sm*MTAP (5, 10, and 25 µg) under a 20 min reaction time (Table 2).

IMER I (4 h immobilization) exhibited substantially higher catalytic activity than IMER II (16 h). One-way ANOVA confirmed significant differences in ADE production between immobilization times ($p < 0.001$), with the 4 h protocol yielding 2.2 to 3.5-fold higher activity across all tested masses. The lower activity observed after 16 h may be attributed to enzyme overloading on the support surface and/or conformational changes resulting from prolonged exposure to immobilization conditions.

Under the 4 h protocol, an immobilization yield of 66.3 ± 6.6% was achieved, indicating efficient glutaraldehyde-mediated covalent coupling between enzyme amine groups and the functionalized magnetic support. These results demonstrate that 4 h is sufficient for effective enzyme attachment while preserving catalytic activity.

Increasing $CoFe_2O_4$@*Sm*MTAP mass led to statistically significant increases in ADE formation ($p < 0.01$); however, the effect was not

Table 1
Mean precision and accuracy values obtained in intra- and inter-day qualification of the ADE quantification method ($n = 5$).

[ADE] (μmol/L)	Precision intra-day (%)	Accuracy intra-day (%)	Precision inter-day 1 (%)	Accuracy inter-day 1 (%)	Precision inter-day 2 (%)	Accuracy inter-day 2 (%)
1.2	4.99	107.3	5.73	103.0	4.04	105.6
40	0.91	98.5	3.63	96.6	0.24	98.9
90	0.48	98.5	0.36	100.6	0.61	100.2

Table 2
Enzymatic activity under different immobilization times and $CoFe_2O_4$@*Sm*MTAP masses.

Immobilization time	Mass of $CoFe_2O_4$@*Sm*MTAP (μg)	Reaction time (min)	[ADE] (μmol/L)
4 h (IMER I)	5	20	12.9
	10	20	15.4
	25	20	21.7
16 h (IMER II)	5	20	3.7
	10	20	7.2
	25	20	8.1

proportional (Table 2). A fivefold increase in support mass (5 to 25 μg) resulted in only ~60% higher product formation. This behavior suggests diffusional limitations, partial inaccessibility of active sites, and/or steric hindrance due to nanoparticle aggregation at higher support concentrations. Because magnetic support and *Sm*MTAP enzyme are high-value materials, this non-proportional gain indicates that simply increasing catalyst mass is not an efficient strategy to enhance assay performance.

To further optimize catalytic conditions, reaction time was evaluated for the lowest and highest support masses (5 and 25 μg) using IMER I (4 h immobilization). Reactions were conducted for 10 and 20 min (Table 3).

In contrast to support mass, reaction time showed a near-linear relationship with ADE production: doubling the reaction time nearly doubled product formation. Two-way ANOVA confirmed a significant main effect of reaction time ($p < 0.001$), with strong linear correlation between time and product formation ($R^2 > 0.95$). This indicates that, within the evaluated range, catalysis remained in a kinetically controlled regime rather than being limited by enzyme saturation.

Considering enzymatic activity, material cost, and assays throughput requirements (particularly for future screening applications), the optimal conditions selected were an immobilization time of 4 h, resulting in an enzyme-to-support mass ratio of 0.133 mg of *Sm*MTAP per mg of $CoFe_2O_4$ magnetic support. The selected catalytic system consisted of 5 μg of $CoFe_2O_4$@*Sm*MTAP and a reaction time of 20 min.

3.4. Stability of $CoFe_2O_4$@SmMTAP

Stability studies of the immobilized enzyme were conducted to evaluate its activity profile over time. Residual activity was expressed as the percentage of ADE formation relative to the activity measured on the day of immobilization (Fig. 1).

A progressive decline in enzymatic activity was observed over the storage period. Activity decreased to 61.1% after two weeks and dropped further to 29.2% by the fourth week. After this point, activity remained relatively stable, with residual activity of approximately 18–20% maintained until the eighth week. This profile suggests that an initial loss of activity occurs during the first weeks of storage, followed by stabilization of a fraction of the immobilized enzyme that remains catalytically active.

Table 3
$CoFe_2O_4$@*Sm*MTAP enzymatic activity under different reaction times.

Immobilization time	Mass of $CoFe_2O_4$@*Sm*MTAP (μg)	Reaction time (min)	[ADE] (μmol/L)
4 h (IMER I)	5	10	3.7
	5	20	7.0
	25	10	6.5
	25	20	11.3

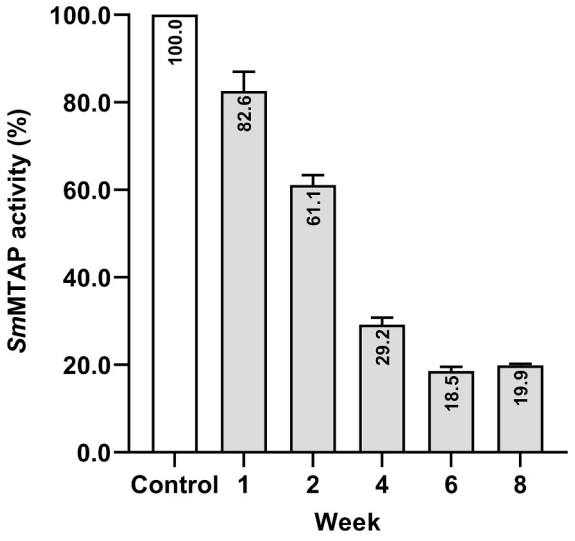

Fig. 1. Stability of immobilized *Sm*MTAP as a function of time.

3.5. Kinetics of $CoFe_2O_4$@SmMTAP

The kinetic parameters of immobilized *Sm*MTAP were determined as part of the functional characterization of the biocatalyst and to define appropriate substrate concentrations for subsequent inhibition and screening assays [38]. The Michaelis-Menten profile obtained for $CoFe_2O_4$@*Sm*MTAP is shown in Fig. 2.

The apparent Michaelis–Menten constant (K_M) was 29.45 ± 7.34 μmol/L, while the maximum reaction velocity (V_{max}) was 5.15 ± 0.39 μmol/L.min. The higher apparent K_M compared with the value reported

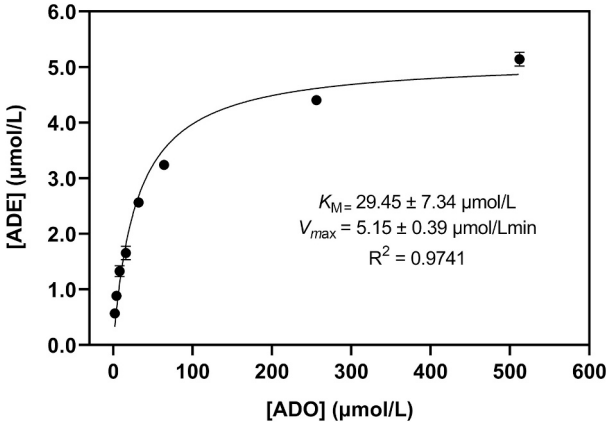

Fig. 2. Michaelis-Menten plot for $CoFe_2O_4$@*Sm*MTAP.

for the free enzyme in the literature (3.14 μmol/L) [26], under the same buffer conditions (100 mmol/L phosphate buffer, pH 7.4), is consistent with typical effects of enzyme immobilization and reflects the influence of mass-transfer limitations, microenvironmental changes, and restricted enzyme mobility on substrate accessibility.

Importantly, the immobilized enzyme maintained a kinetic profile that follows Michaelis-Menten behavior, confirming preservation of its catalytic function after covalent attachment to the support. In this context, the apparent K_M value should be interpreted as an operational parameter of the immobilized system under the selected assay conditions.

From an analyticalperspective, determination of K_M is essential for rational screening assay design. Substrate concentrations can be selected relative to this value to ensure sensitivity to competitive inhibitors, since excessively high substrate levels may mask inhibition effects by favoring formation of the enzyme–substrate complex.

3.6. Reusability of $CoFe_2O_4$@SmMTAP

The operational reusability of $CoFe_2O_4$@*Sm*MTAP was evaluated over consecutive catalytic cycles to assess its suitability for repeated analytical use. Residual activity in each cycle was expressed relative to the activity measured in the first reaction (Fig. 3).

The immobilized enzyme retained approximately 50% of its initial activity after seven cycles, decreasing to about 25% by the tenth cycle. This progressive decline likely reflects not only partial enzyme inactivation, but also physical losses of magnetic support during handling, such as incomplete particle collection and adsorption of nanoparticles to microtube walls.

From an analytical perspective, activity levels below 25% of the initial value fall outside the range considered adequate for reliable inhibition measurements. Therefore, $CoFe_2O_4$@*Sm*MTAP can be reused for up to eight reaction cycles without compromising assay performance.

To ensure reproducibility, the reusability study was conducted in parallel using two independently prepared immobilized enzyme batches, which showed comparable activity decay profiles.

3.7. Inhibitor screening assays

The developed LC-based assay was applied to screen natural product extracts as potential sources of *Sm*MTAP inhibitors. Inhibition was expressed as the percentage reduction in ADE formation relative to the negative control, in which the extract was replaced by the corresponding solvent used for its preparation. The screening included eight natural extracts obtained from different parts of *Hymenaea stigonocarpa* and *Moringa oleifera* (Fig. 4).

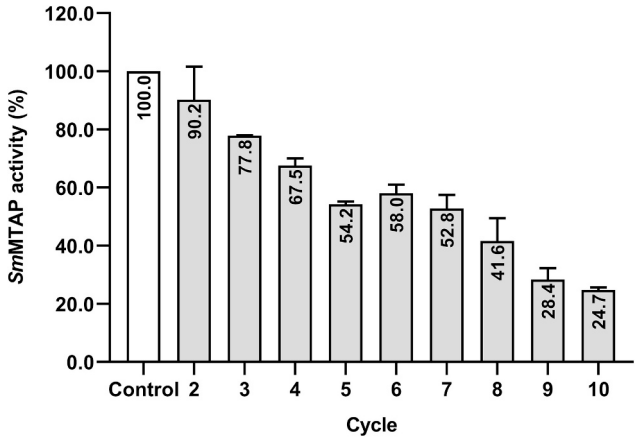

Fig. 3. Reusability profile of $CoFe_2O_4$@*Sm*MTAP over consecutive reaction cycles.

In this assay *H. stigonocarpa* extracts emerged as the most interesting source of inhibitors. The ethanolic stem extract (HS-EEC) exhibited 92.8% inhibition, followed by the ethanolic fruit peel extract (HS-EECF) with 89.4%, and the ethanolic root extract (HS-EER) with 75.1% inhibition at 200 μg/mL. No interference from extract matrix components was observed in ADE quantification.

Based on the screening criterion of ≥70% inhibition at the evaluated concentration, HS-EEC, HS-EECF, and HS-EER were selected for further IC_{50} determination.

3.8. IC_{50} assays

IC_{50} values were determined for the three selected extracts (HS-EEC, HS-EECF, and HS-EER) to further characterize their inhibitory potency. The results are summarized in Table 4.

The experimental data were fitted to a sigmoidal dose–response model, and the corresponding curves are shown in Figs. S5-S7. Among the evaluated samples, HS-EEC exhibited the highest inhibitory potency, with an IC_{50} of 8.29 ± 0.94 μg/mL, followed by HS-EER and HS-EECF. These results confirm HS-EEC as the most promising source of *Sm*MTAP inhibitors, supporting its selection for subsequent investigations, including AS-MS assays, *Sm*MTAP inhibition profiling, and dereplication.

3.9. Affinity selection-mass spectrometry (AS-MS)

AS-MS is a powerful strategy for the rapid identification of enzyme ligands directly from crude natural product extracts [39–41]. In this study, AS-MS was employed to identify *Sm*MTAP ligands directly from HS-EEC extract, using the $CoFe_2O_4$@*Sm*MTAP to capture and separate the enzyme-ligand complex from the crude extract [18,42]. Comparison of UHPLC-HRMS profiles obtained from active and inactive enzyme assays revealed six enriched ligands in the positive ionization mode, with affinity ratios (AR) ranging from 1.45 to 2.89 (Figs. S8-S13) and retention times between 32.3 and 41.2 min (Fig. 5 and Table 5). Additionally, ligand 6 (rt 41.2 min) and ligand 4 (rt 36.8 min) were also detected in negative ionization mode as formate adduct at *m/z* 551.2188 and 431.1706, respectively.

Structural annotation was attempted using the dereplication criteria described in Section 2.14. Among the six candidates, only ligand 6 (rt

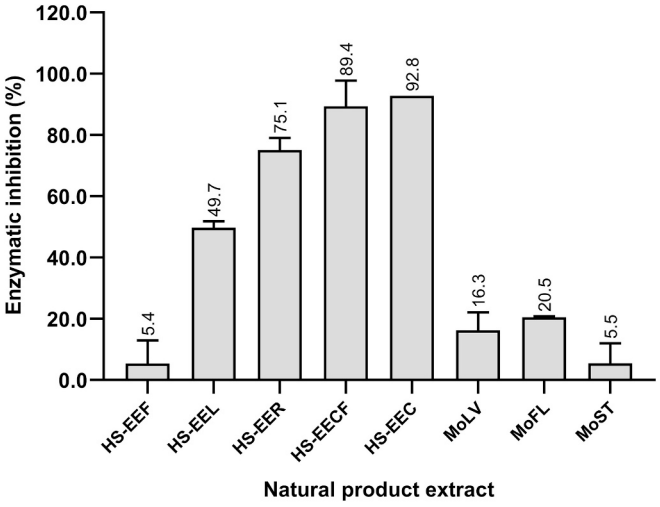

Fig. 4. Inhibitory activity of natural product extracts at 200 μg/mL. The evaluated samples included *H. stigonocarpa* ethanolic flowers (HS-EEF), leaves (HS-EEL), roots (HS-EER), fruit peel (HS-EECF) and stem (HS-EEC) extracts, as well as *M. oleifera* hydroethanolic stem (MoST), leaves (MoLV) and flowers (MoFL) extracts.

Table 4
Most active extracts identified in the screening assays and their corresponding IC_{50} values.

Extract	Inhibition at 200 μg/mL (%)	IC_{50} (μg/mL)
HS-EEC	92.8 ± 0.1	8.29 ± 0.94
HS-EECF	89.4 ± 5.9	62.17 ± 7.67
HS-EER	75.1 ± 2.8	24.06 ± 6.72

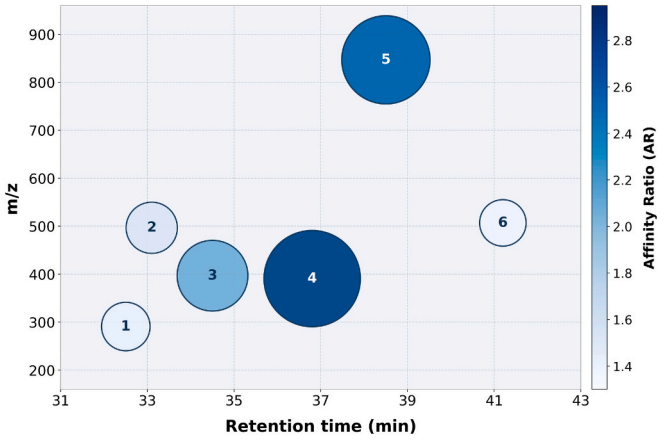

Fig. 5. Bubble chart representing the six *Sm*MTAP ligands selectively enriched from the ethanolic stem extract of *H. stigonocarpa* (HS-EEC) by affinity selection–mass spectrometry (AS-MS). Each bubble corresponds to one ligand (numbered 1–6); the horizontal axis indicates retention time (min), the vertical axis indicates the observed *m/z* $[M + H]^+$, bubble size is proportional to the affinity ratio (AR), and bubble color encodes AR intensity on a continuous scale from light blue (low AR) to dark blue (high AR). AR values >1.3 were considered indicative of selective binding to the active enzyme. (For interpretation of the references to color in this figure legend, the reader is referred to the web version of this article.)

Table 5
Summary of *Sm*MTAP ligands identified in HS-EEC by AS-MS, including retention time, affinity ratio (AR), observed *m/z*, and MS/MS fragment ions.

Entry	Retention time (min)	Affinity ratio	*m/z* $[M + H]^+$	Fragments
1	32.3	1.45	290.2685	228.2315; 184.2041; 272.2605
2	33.1	1.57	494.4053	388.3417; 344.3177; 345.3191; 300.2919
3	34.4	2.37	390.3581	328.3203; 391.3604; 284.2939; 329.3243;
4	36.8	2.89	387.1802	105.0693; 121.0649; 93.0702; 106.0732
5	38.7	2.42	846.4441	415.2122; 281.1370; 119.0854; 437.1951;
6	41.2	1.79	507.2282	238.1225; 256.1327; 224.1060; 239.1252;

41.2 min, *m/z* 507.2282 $[M + H]^+$, AR = 1.79) showed tentative library match to asperphenamate (cosine score 0.94, Δ*m/z* 0.59 ppm), a dipeptide ester of phenylalanine and benzoic acid previously reported from fungal sources [43]. This assignment should be interpreted cautiously, as it is based on spectral matching only and does not provide structural confirmation. Accordingly, it may correspond to a minor constituent, a contaminant, or a compound of non-plant origin. This result highlights the ability of AS-MS to capture high-affinity binders regardless of their biosynthetic origin within a complex matrix. The remaining ligands did not meet the confidence criteria for annotation and therefore remain unassigned, requiring further isolation and spectroscopic characterization.

3.10. Inhibitory profile of HS-EEC

To associate chromatographic features with functional inhibition and complement the AS-MS findings, HS-EEC was subjected to analytical-scale HPLC microfractionation under the optimized chromatographic conditions described in Section 2.14 (Fig. S14). The 29.0 to 44.0 min interval was selected, as it encompasses the elution window of all six *Sm*MTAP ligands (32.3–41.2 min) detected in the AS-MS assays. After fraction collection, solvent removal, and reconstitution in assay buffer, each microfraction was evaluated for *Sm*MTAP inhibitory activity. The inhibition percentages were plotted against retention time, generating the inhibitory chromatographic profile (biochromatogram) shown in Fig. 6.

A pronounced bioactive region was observed between 30.75 and 33.0 min, with inhibition values ranging from 75.4% to 94.3% and a maximum at 31.5 min. This interval overlaps with the elution range of ligands 1 (rt 32.3 min, AR = 1.45) and 2 (rt 33.1 min, AR = 1.57) detected in the AS-MS assay. These results prioritize the 30.75–33.0 min region for targeted isolation and suggest that ligands 1 and/or 2 may contribute to the observed inhibitory activity, although co-eluting constituents cannot be excluded.

In contrast, a sharp decrease in inhibitory activity was observed from 34.0 min onwards, with inhibition values remaining below 30% during the evaluated interval (34.0–44.0 min). This region encompasses ligands 3–6 (rt 34.4–41.2 min), which, despite showing selective affinity for the active enzyme in the AS-MS assay, were not associated with significant inhibition in the biochromatogram.

A direct correlation between affinity (expressed as AR values obtained by AS-MS) and the inhibitory response observed in the activity assay is not necessarily expected, given the distinct nature of these approaches. AS-MS detects ligand–protein binding events regardless of their functional outcome, whereas the bioassay specifically reflects the ability of a compound to interfere with catalytic activity. In this context, non-productive binding must be considered, as compounds may interact with *Sm*MTAP without affecting its catalytic function. Additionally, ligand binding may occur at sites distinct from the catalytic active site, including allosteric sites that do not modulate enzyme activity under the assay conditions employed, or surface-exposed regions that are not functionally relevant.

The AR provides a relative estimation of binding, whereas a more rigorous quantification would require determination of dissociation constants (K_d) for individual ligands. However, in complex matrices such as plant extracts, this type of analysis is challenging due to the presence of multiple constituents at varying concentrations competing for interaction with the target.

Furthermore, the analytical-scale microfractionation approach is subject to detection limits that may hinder the identification of low-abundance bioactive compounds. Notably, asperphenamate (ligand 6, rt. 41.2 min, AR = 1.79) eluted in a region of minimal inhibitory activity in the biochromatogram, suggesting that its interaction with *Sm*MTAP may not translate into measurable catalytic inhibition under the evaluated conditions. While AS-MS can detect ligands at low concentrations, the inhibitory response is concentration-dependent. Therefore, weak inhibitors or low-abundance compounds may not produce a measurable effect in the bioassay, leading to discrepancies between observed binding and inhibition profile.

Taken together, these considerations highlight the complementary nature of AS-MS and functional bioassays in the characterization of bioactive compounds from complex natural matrices. Although individual validation of isolated ligands was not performed in this study, the biochromatogram provides a rational basis for targeted isolation in future work. In this context, ligands 1 and 2, eluting between 32.3 and 33.1 min, represent the most promising candidates for further investigation studies aiming to enrich and isolate these fractions for structural elucidation and individual bioactivity confirmation. It should also be noted that, given the material and time constraints inherent to

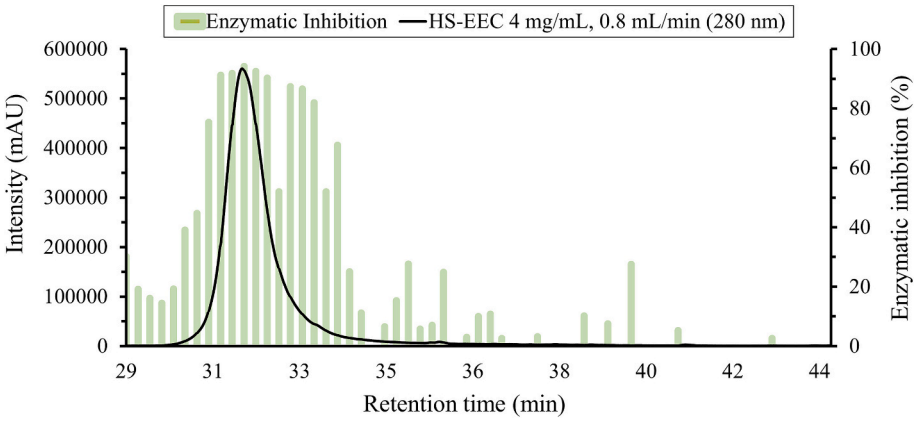

Fig. 6. Inhibitory profile (biochromatogram) of HS-EEC monitored at 280 nm in the range of 29 to 44 min.

analytical-scale microfractionation, each of the 60 collected fractions was evaluated in a single measurement. However, the resulting inhibitory trends are clear and regionally consistent.

3.11. Dereplication of HS-EEC constituents

UHPLC–HRMS analysis of HS-EEC (Figs. S15 and S16) enabled the putative annotation of 23 constituents, including 16 detected in positive ionization mode and 7 detected exclusively in negative ionization mode (Tables S2 and S3).

The annotated features were distributed across several metabolite classes, with a predominance of polyphenolic constituents such as flavan-3-ols (epicatechin, catechin), proanthocyanidins (procyanidin B1, B2, A1, and C1), flavonols (quercitrin, isoquercitrin, 3-*O*-methylquercetin), a flavone (vitexin), a chalcone (coatlin A), a flavanone glycoside, and an isoflavone (odoratin). Phenylpropanoids were also represented, including neochlorogenic acid, 1,3-dicaffeoylquinic acid, and a phenylpropanoid glycoside ester. Additional putative annotations included lignans (an aryltetralin lignan glycoside and dihydrodehydrodiconiferyl alcohol), a diterpenoid (clerodane-type), a triterpenoid (oleanolic acid), and a flavone-type compound (acacetin).

Comparison with published phytochemical data for *H. stigonocarpa* (Table S4) indicates that most of the annotated constituents have not been previously reported for this species, representing a meaningful expansion of its known chemical profile. Among the exceptions, epicatechin, procyanidin C1, and quercitrin have been described in stem bark extracts of *H. stigonocarpa* [44,45], lending additional confidence to the spectral matching approach employed.

It should be noted that all annotations are putative and based on spectral library matching with cosine scores $\geq$0.70 and mass errors $\leq$15 ppm, as appropriate for a Q-TOF instrument. Structural confirmation for individual constituents will require isolation and full spectroscopic characterization. It is important to note that the dereplication data presented in this section aim to expand the known phytochemical profile of *H. stigonocarpa* and provide chemical context for the extract, rather than to identify the compounds responsible for the observed *Sm*MTAP inhibitory activity. As discussed in Sections 3.9 and 3.10, the most bioactive compounds (ligands 1 and 2, eluting at 32.3 and 33.1 min) remain structurally uncharacterized, and a direct link between the annotated constituents and the inhibitory profile cannot be established at this stage.

4. Conclusions

This study established a covalent immobilization strategy for *Sm*MTAP onto $CoFe_2O_4$ magnetic nanoparticles and validated the resulting $CoFe_2O_4$@*Sm*MTAP system as a reusable bioanalytical platform for enzyme activity monitoring and inhibitor screening. The optimized bioreactor (66.3 $\pm$ 6.6% immobilization efficiency) preserved Michaelis–Menten behavior, retained >60% activity over two weeks, and remained operational for at least seven consecutive cycles, significantly reducing enzyme consumption compared to solution-based assays.

The validated HPLC-DAD method provided selective and interference-free quantification of adenine, enabling reliable screening of complex natural product extracts. Application to eight extracts from *H. stigonocarpa* and *M. oleifera* allowed clear discrimination of inhibitory samples and quantitative potency ranking (IC_{50} 8.29–62.17 μg/mL).

Following IC_{50} determination, AS-MS assays identified six *Sm*MTAP ligands in the most active extract (HS-EEC). Analytical-scale microfractionation subsequently generated an *Sm*MTAP inhibitory chromatographic profile that localized the principal bioactive window to the 30.75–33.0 min retention time region. Correlation of both datasets revealed that two of the AS-MS-identified ligands eluted within this high-inhibition window, supporting their prioritization for targeted isolation Finally, UHPLC–HRMS dereplication enabled the putative annotation of 23 constituents and expanded the known chemical profile of *H. stigonocarpa*.

It should be acknowledged that the absence of a known *Sm*MTAP inhibitor as a positive control represents a limitation of the present study, reflecting the overall underexplored nature of this enzyme as a drug target. The only inhibitor reported in the literature, 5′-deoxy-5′-chloroformycin A [16], is not commercially available. Future work will focus on targeted enrichment, isolation, and full structural elucidation of the constituents eluting within the 30.75–33.0 min window, followed by confirmation of their individual inhibitory potency against *Sm*MTAP. Overall, the integrated immobilized-enzyme, AS-MS, inhibition profiling, and HRMS-based workflow constitutes a robust and efficient strategy for target-directed screening in complex natural product libraries.

Declaration of generative Ai and Ai-assisted technologies in the manuscript preparation process

During the preparation of this work, the authors used Grammarly to assist with language refinement and writing clarity, and Claude (Anthropic) to assist in the elaboration of Fig. 5. After using these tools, the authors reviewed and edited the content as needed and take full responsibility for the content of the published article.

CRediT authorship contribution statement

Lucas G. do Amaral: Writing – review & editing, Writing – original draft, Validation, Methodology, Investigation, Formal analysis, Data curation. **Miguel F.S. de Abreu:** Writing – original draft, Validation, Methodology, Investigation, Formal analysis. **Renato C.S. Lessa:**

Writing – original draft, Supervision, Methodology, Investigation, Formal analysis. **Pamella C.O. de Oliveira:** Writing – original draft, Supervision, Methodology, Investigation, Formal analysis. **Magali S. Amorim:** Resources, Methodology, Investigation, Formal analysis. **Jorge L.S. Simão:** Resources, Formal analysis. **Martin Albino:** Supervision, Resources, Investigation. **Humberto d'Muniz Pereira:** Visualization, Resources, Investigation. **Claudio Sangregorio:** Supervision, Resources, Investigation. **Vanessa G.P. Severino:** Writing – review & editing, Writing – original draft, Supervision, Resources, Methodology, Investigation, Formal analysis. **Marcela C. de Moraes:** Writing – review & editing, Writing – original draft, Visualization, Supervision, Resources, Project administration, Methodology, Investigation, Funding acquisition, Formal analysis, Data curation, Conceptualization.

Declaration of competing interest

The authors declare that they have no known competing financial interests or personal relationships that could have appeared to influence the work reported in this paper.

Acknowledgements

We thank Centro de Espectrometria de Massas de Biomoléculas (CEMBIO) for their technical support and for providing access to their facilities. This investigation was supported by the Conselho Nacional de Desenvolvimento Científico e Tecnológico (CNPq) (grants 408050/2025-0 and 305911/2025-2), the Coordenação de Aperfeiçoamento de Pessoal de Nível Superior – Brasil (CAPES) – Finance Code 001, and Fundação Carlos Chagas Filho de Amparo à Pesquisa do Estado do Rio de Janeiro (FAPERJ) [grants E-26/210.017/2024, E-26/200.172/2023, E-26/211.337/2021, E-26/202.111/2025, and E-26/210.547/2025].

Appendix A. Supplementary data

Supplementary data to this article can be found online at https://doi.org/10.1016/j.bioorg.2026.109993.

Data availability

Data will be made available on request.

References

[1] A.M. Ibrahim, Strategies for schistosomiasis control targeting snail intermediate hosts: a review, Biologia (Bratisl). (2025), https://doi.org/10.1007/s11756-025-01930-7.
[2] B. Chala, Advances in diagnosis of schistosomiasis: focus on challenges and future approaches, Int. J. Gen. Med. 16 (2023) 983–995, https://doi.org/10.2147/IJGM.S391017.
[3] Portal Gov.br, Esquistossomose, Ministério Da Saúde, 2026. https://www.gov.br/saude/pt-br/assuntos/saude-de-a-a-z/e/esquistossomose (accessed March 15, 2026).
[4] F.W.B. Salviano, J.E.B.A. Vieira, J.P. dos S. Neto, A.V.C. Machado, A.É. L. Grangeiro, B.C.M. Da Silva, B.N. Lima, M.R. Lopes e Silva, C.G.L. Da Silva, M. do S.V. dos Santos, Epidemiology of schistosomiasis in Brazil: a retrospective study, Concilium 23 (2023) 413–431, https://doi.org/10.53660/CLM-1861-23M60.
[5] V.B.R. da Silva, B.R.K.L. Campos, J.F. de Oliveira, J.L. Decout, M. do Carmo Alves de Lima, Medicinal chemistry of antischistosomal drugs: praziquantel and oxamniquine, Bioorg. Med. Chem. 25 (2017) 3259–3277, https://doi.org/10.1016/J.BMC.2017.04.031.
[6] S.N. Alwan, A.B. Taylor, J. Rhodes, M. Tidwell, S.F. McHardy, P.T. LoVerde, Oxamniquine derivatives overcome Praziquantel treatment limitations for Schistosomiasis, PLoS Pathog. 19 (2023) e1011018, https://doi.org/10.1371/journal.ppat.1011018.
[7] C.M. Thomas, D.J. Timson, The mechanism of action of praziquantel: can new drugs exploit similar mechanisms? Curr. Med. Chem. 27 (2020) 676–696, https://doi.org/10.2174/0929867325666180926145537.
[8] A.W. Senft, R.P. Miech, P.R. Brown, D.G. Senft, Purine metabolism in Schistosoma mansoni, Int. J. Parasitol. 2 (1972) 249–260, https://doi.org/10.1016/0020-7519(72)90013-6.
[9] A.W. Senft, G.W. Crabtree, Purine metabolism in the schistosomes: potential targets for chemotherapy, Pharmacol. Ther. 20 (1983) 341–356, https://doi.org/10.1016/0163-7258(83)90031-1.
[10] H.F. Dovey, J.H. McKerrow, C.C. Wang, Purine salvage in Schistosoma mansoni schistosomules, Mol. Biochem. Parasitol. 11 (1984) 157–167, https://doi.org/10.1016/0166-6851(84)90062-8.
[11] M.H. el Kouni, Potential chemotherapeutic targets in the purine metabolism of parasites, Pharmacol. Ther. 99 (2003) 283–309, https://doi.org/10.1016/S0163-7258(03)00071-8.
[12] J.R.T. de Souza, Determinação estrutural e funcional da enzima 5′-deoxi-5′-metiltioadenosina Fosforilase de Schistosoma mansoni, University of São Paulo (2012), https://doi.org/10.11606/D.76.2012.tde-01062012-171148.
[13] L. Pagiatto, Modulação da infecção murina pelas enzimas recombinantes MTAP e APRT de Schistosoma mansoni, Dissertation, Federal University of São Carlos, 2016. https://repositorio.ufscar.br/handle/20.500.14289/7535 (accessed April 19, 2026).
[14] A.W. Senft, G.W. Crabtree, K.C. Agarwal, E.M. Scholar, R.P. Agarwal, R.E. Parks, Pathways of nucleotide metabolism in Schistosoma mansoni—III, Biochem. Pharmacol. 22 (1973) 449–458, https://doi.org/10.1016/0006-2952(73)90286-4.
[15] F.L. Meyskens, H.E. Williams, Adenosine metabolism in human erythrocytes, Biochimica et Biophysica acta (BBA) - nucleic acids and protein Synthesis 240 (1971) 170–179, https://doi.org/10.1016/0005-2787(71)90654-X.
[16] T.M. Savarese, M.H. el Kouni, Isolation and substrate specificity of an adenine nucleoside phosphorylase from adult Schistosoma mansoni, Mol. Biochem. Parasitol. 194 (2014) 44–47, https://doi.org/10.1016/j.molbiopara.2014.04.008.
[17] N.R. Mohamad, N.H.C. Marzuki, N.A. Buang, F. Huyop, R.A. Wahab, An overview of technologies for immobilization of enzymes and surface analysis techniques for immobilized enzymes, Biotechnol. Biotechnol. Equip. 29 (2015) 205–220, https://doi.org/10.1080/13102818.2015.1008192.
[18] P.C.O. Ximenes, C.A. de Oliveira, M.C. Wegermann, de Moraes, Magnetic particles for enzyme immobilization: a versatile support for ligand screening, J. Pharm. Biomed. Anal. 204 (2021) 114286, https://doi.org/10.1016/j.jpba.2021.114286.
[19] A. López-Ortega, E. Lottini, C. de J. Fernández, C. Sangregorio, Exploring the magnetic properties of cobalt-ferrite nanoparticles for the development of a rare-earth-free permanent magnet, Chem. Mater. 27 (2015) 4048–4056, https://doi.org/10.1021/acs.chemmater.5b01034.
[20] I.A. Trindade Ximenes, M. Albino, C. Sangregorio, Q.B. Cass, M.C. de Moraes, On-flow magnetic particle activity assay for the screening of human purine nucleoside phosphorylase inhibitors, J. Chromatogr. A 1663 (2022) 462740, https://doi.org/10.1016/J.CHROMA.2021.462740.
[21] M. Ribani, C.B.G. Bottoli, C.H. Collins, I.C.S.F. Jardim, L.F.C. Melo, Validação em métodos cromatográficos e eletroforéticos, Quim Nova 27 (2004) 771–780, https://doi.org/10.1590/S0100-40422004000500017.
[22] P.S. Tresina, M.S. Selvam, A. Rajesh, A. Doss, V.R. Mohan, Natural products in drug discovery: approaches and development, J. Pharm. Res. Int. (2021) 93–110, https://doi.org/10.9734/jpri/2021/v33i35A31879.
[23] Z. Peng, J. Lu, K. Liu, L. Xie, Y. Wang, C. Cai, D. Yang, J. Xi, C. Yan, X. Li, M. Shi, Hypericin as a promising natural bioactive naphthodianthrone: a review of its pharmacology, pharmacokinetics, toxicity, and safety, Phytother. Res. 37 (2023) 5639–5656, https://doi.org/10.1002/ptr.8011.
[24] N.B. Cech, N.H. Oberlies, From plant to cancer drug: lessons learned from the discovery of taxol, Nat. Prod. Rep. 40 (2023) 1153–1157, https://doi.org/10.1039/D3NP00017F.
[25] S. Xie, F. Zhan, J. Zhu, S. Xu, J. Xu, The latest advances with natural products in drug discovery and opportunities for the future: a 2025 update, Expert Opin. Drug Discov. (2025), https://doi.org/10.1080/17460441.2025.2507382.
[26] J.R. Torini, J. Brandão-Neto, R. DeMarco, H.D. Pereira, Crystal structure of Schistosoma mansoni adenosine phosphorylase/5′-Methylthioadenosine phosphorylase and its importance on adenosine salvage pathway, PLoS Negl. Trop. Dis. 10 (2016) e0005178, https://doi.org/10.1371/journal.pntd.0005178.
[27] P.C.O. de Oliveira, P.R.C. Medeiros, B.C.B. Marques, J.L.S. Simão, M. Albino, V.G. P. Severino, C. Sangregorio, L.W. Tinoco, M.C. de Moraes, Identification of novel leishmania donovani nucleoside hydrolase inhibitors from Banisteriopsis laevifolia using affinity selection-mass spectrometry, ACS Omega 10 (2025) 23249–23259, https://doi.org/10.1021/acsomega.5c01613.
[28] R.A. de Faria, P.C.O. Oliveira, M.D.P. de Carvalho, B.S. Peixoto, V.G.P. Severino, L. W. Tinoco, S.V. Rodrigues, M.C. de Moraes, High-resolution inhibition profiling and ligand fishing for screening of nucleoside hydrolase ligands in Moringa oleifera Lamarck, J. Pharm. Biomed. Anal. 211 (2022) 114614, https://doi.org/10.1016/j.jpba.2022.114614.
[29] S.C. Gill, P.H. von Hippel, Calculation of protein extinction coefficients from amino acid sequence data, Anal. Biochem. 182 (1989) 319–326, https://doi.org/10.1016/0003-2697(89)90602-7.
[30] P. Kießling, G.K.E. Scriba, F. Süß, G. Werner, H. Knoth, M. Hartmann, Development and validation of a high-performance liquid chromatography assay and a capillary electrophoresis assay for the analysis of adenosine and the degradation product adenine in infusions, J. Pharm. Biomed. Anal. 36 (2004) 535–539, https://doi.org/10.1016/j.jpba.2004.07.005.
[31] Brasil Agência Nacional de Vigilância Sanitária (ANVISA), Resolução da Diretoria Colegiada – RDC nº 166, de 24 de julho de 2017, Brasil. https://www.in.gov.br/materia/-/asset_publisher/Kujrw0TZC2Mb/content/id/19194581/do1-2017-07-25-resolucao-rdc-n-166-de-24-de-julho-de-2017-19194412, 2017 (accessed February 24, 2026).
[32] Brasil Agência Nacional de Vigilância Sanitária (ANVISA), Resolução da Diretoria Colegiada – RDC nº 27, de 17 de maio de 2012, Brasil. https://bvsms.saude.gov.br/bvs/saudelegis/anvisa/2012/rdc0027_17_05_2012.html, 2012 (accessed February 24, 2026).
[33] J. Miller, J. Miller, Statistics for Analytical Chemistry, 3rd ed., Ellis Horwood Ltd, 1993.

[34] A.F. Monteiro, J.M. Batista, M.A. Machado, R.P. Severino, E.W. Blanch, V. S. Bolzani, P.C. Vieira, V.G.P. Severino, Structure and absolute configuration of diterpenoids from Hymenaea stigonocarpa, J. Nat. Prod. 78 (2015) 1451–1455, https://doi.org/10.1021/acs.jnatprod.5b00166.

[35] R. Schmid, S. Heuckeroth, A. Korf, A. Smirnov, O. Myers, T.S. Dyrlund, R. Bushuiev, K.J. Murray, N. Hoffmann, M. Lu, A. Sarvepalli, Z. Zhang, M. Fleischauer, K. Dührkop, M. Wesner, S.J. Hoogstra, E. Rudt, O. Mokshyna, C. Brungs, K. Ponomarov, L. Mutabdžija, T. Damiani, C.J. Pudney, M. Earll, P. O. Helmer, T.R. Fallon, T. Schulze, A. Rivas-Ubach, A. Bilbao, H. Richter, L.-F. Nothias, M. Wang, M. Orešič, J.-K. Weng, S. Böcker, A. Jeibmann, H. Hayen, U. Karst, P.C. Dorrestein, D. Petras, X. Du, T. Pluskal, Integrative analysis of multimodal mass spectrometry data in MZmine 3, Nat. Biotechnol. 41 (2023) 447–449, https://doi.org/10.1038/s41587-023-01690-2.

[36] M. Wang, J.J. Carver, V.V. Phelan, L.M. Sanchez, N. Garg, Y. Peng, D.D. Nguyen, J. Watrous, C.A. Kapono, T. Luzzatto-Knaan, C. Porto, A. Bouslimani, A.V. Melnik, M.J. Meehan, W.-T. Liu, M. Crüsemann, P.D. Boudreau, E. Esquenazi, M. Sandoval-Calderón, R.D. Kersten, L.A. Pace, R.A. Quinn, K.R. Duncan, C.-C. Hsu, D.J. Floros, R.G. Gavilan, K. Kleigrewe, T. Northen, R.J. Dutton, D. Parrot, E.E. Carlson, B. Aigle, C.F. Michelsen, L. Jelsbak, C. Sohlenkamp, P. Pevzner, A. Edlund, J. McLean, J. Piel, B.T. Murphy, L. Gerwick, C.-C. Liaw, Y.-L. Yang, H.-U. Humpf, M. Maansson, R.A. Keyzers, A.C. Sims, A.R. Johnson, A.M. Sidebottom, B.E. Sedio, A. Klitgaard, C.B. Larson, C.A. Boya P, D. Torres-Mendoza, D.J. Gonzalez, D. B. Silva, L.M. Marques, D.P. Demarque, E. Pociute, E.C. O'Neill, E. Briand, E.J. N. Helfrich, E.A. Granatosky, E. Glukhov, F. Ryffel, H. Houson, H. Mohimani, J. J. Kharbush, Y. Zeng, J.A. Vorholt, K.L. Kurita, P. Charusanti, K.L. McPhail, K. F. Nielsen, L. Vuong, M. Elfeki, M.F. Traxler, N. Engene, N. Koyama, O.B. Vining, R. Baric, R.R. Silva, S.J. Mascuch, S. Tomasi, S. Jenkins, V. Macherla, T. Hoffman, V. Agarwal, P.G. Williams, J. Dai, R. Neupane, J. Gurr, A.M.C. Rodríguez, A. Lamsa, C. Zhang, K. Dorrestein, B.M. Duggan, J. Almaliti, P.-M. Allard, P. Phapale, L.-F. Nothias, T. Alexandrov, M. Litaudon, J.-L. Wolfender, J.E. Kyle, T. O. Metz, T. Peryea, D.-T. Nguyen, D. VanLeer, P. Shinn, A. Jadhav, R. Müller, K. M. Waters, W. Shi, X. Liu, L. Zhang, R. Knight, P.R. Jensen, B.Ø. Palsson, K. Pogliano, R.G. Linington, M. Gutiérrez, N.P. Lopes, W.H. Gerwick, B.S. Moore, P. C. Dorrestein, N. Bandeira, Sharing and community curation of mass spectrometry data with global natural products social molecular networking, Nat. Biotechnol. 34 (2016) 828–837, https://doi.org/10.1038/nbt.3597.

[37] H.M. Kalckar, Differential spectrophotometry of purine compounds by means of specific enzymes: i. determination of hydroxypurine compounds, J. Biol. Chem. 167 (1947) 429–443, https://doi.org/10.1016/S0021-9258(17)30997-3.

[38] C. Anchau Wegermann, E. Santana Bezerra, I. Gomes de Macedo Sant'Anna, P.C. Ortega De Oliveira, R. da Costa Silva, T. Rocco Machado, L. Wanderley Tinoco, M. C.B. Vieira de Souza, P. Pascutti, F. da C. Santos Boechat, M.C. de Moraes, Insights into nucleoside hydrolase from *Leishmania donovani* inhibition: a new bioaffinity chromatography-based screening assay and docking studies, Bioorg. Chem. 146 (2024) 107302, https://doi.org/10.1016/j.bioorg.2024.107302.

[39] D.A. Annis, E. Nickbarg, X. Yang, M.R. Ziebell, C.E. Whitehurst, Affinity selection-mass spectrometry screening techniques for small molecule drug discovery, Curr. Opin. Chem. Biol. 11 (2007) 518–526, https://doi.org/10.1016/j.cbpa.2007.07.011.

[40] B.S. do Amaral, M.C. de Moraes, C.L. Cardoso, Q.B. Cass, Affinity selection mass spectrometry (AS-MS) for prospecting ligands in natural product libraries, Front. Nat. Prod. 4 (2025), https://doi.org/10.3389/fntpr.2025.1562501.

[41] P.C.O. de Oliveira, B.S. do Amaral, C.L. Cardoso, Q.B. Cass, M.C. De Moraes, Breaking the boundaries of affinity selection-mass spectrometry: from ligand screening to target-ligand interaction insights, J. Pharm. Anal. (2025) 101379, https://doi.org/10.1016/J.JPHA.2025.101379.

[42] L.A. Miranda de Souza Duarte-Filho, P.C. Ortega de Oliveira, C.E. Yanaguibashi Leal, M.C. de Moraes, L. Picot, Ligand fishing as a tool to screen natural products with anticancer potential, J. Sep. Sci. 46 (2023), https://doi.org/10.1002/jssc.202200964.

[43] K. Subko, X. Wang, F.H. Nielsen, T. Isbrandt, C.H. Gotfredsen, M.C. Ramos, T. Mackenzie, F. Vicente, O. Genilloud, J.C. Frisvad, T.O. Larsen, Mass spectrometry guided discovery and Design of Novel Asperphenamate Analogs from Penicillium astrolabium reveals an extraordinary NRPS flexibility, Front. Microbiol. 11 (2021), https://doi.org/10.3389/fmicb.2020.618730.

[44] K. de S. Farias, S.A. Auharek, A.L. Cunha-Laura, J.M.E. de Souza, G.A. Damasceno-Junior, M.C. Toffoli-Kadri, W.F. de Oliveira Filiú, E. dos A. dos Santos, M.R. Chang, C.A. Carollo, Adulteration and contamination of commercial sap of *Hymenaea* species, Evid. Based Complement. Alternat. Med. 2017 (2017), https://doi.org/10.1155/2017/1919474.

[45] G.S. Dimech, Estudo fitoquímico e antimicrobiano da casca do caule de Hymenaea stigonocarpa, Federal University of Pernambuco, Thesis, 2014 https://repositorio.ufpe.br/handle/123456789/22219 (accessed March 1, 2026).